Lateral Graphene–hBCN Heterostructures as a Platform for Fully Two-Dimensional Transistors

Gianluca Fiori,[†],[*] Alessandro Betti,[†] Samantha Bruzzone,[†] and Giuseppe Iannaccone[†,‡]

[†]Dipartimento di Ingegneria dell'Informazione, Università di Pisa, Via G. Caruso 16, 56122 Pisa, Italy, and [‡]IEIIT-CNR

Hopes of high-performance graphene-based integrated circuits are at high risk. They are fueled by compatibility with silicon technology, record-high mobility of electron and holes, and the quasi-ideal electrostatics enabled by the ultimate thinness of graphene monolayers. However, both experiments[1,2] and simulation-based technology explorations have shown that field effect transistors (FETs) with a graphene-based channel cannot be effectively switched off because the energy gap of the channel is either too small, or not reliable.[3–5]

Recent experiments[6] have shown the possibility of fabricating two-dimensional hybrid structures consisting of intercalated carbon and hBCN (hexagonal boron carbon nitrogen) domains, whose electronic and mechanical properties can be tuned by varying the relative fractions of the three elements. Though transport experiments are not yet available, we believe such structures are extremely promising and can open new routes for graphene nanoelectronics, since hybrid hBCN-graphene can overcome the energy-gap limitation of graphene. Indeed, proper use of hBCN domains can allow the suppression of the ambipolar behavior of graphene FETs, blocking the flow of one type of carriers, and to fully modulate current due to carriers of the other type.

Here, we explore the possibility offered by planar hBCN–graphene heterostructures for truly planar nanoscale devices, using a multiscale simulation approach coupling *ab initio* simulations based on density-functional theory (DFT) with quantum transport device simulations based on the non-equilibrium Green's functions (NEGF) formalism and on an atomistic tight-binding (TB) Hamiltonian.

We consider fully coherent transport and defectless devices (*e.g.*, ideal graphene–hBCN interface), therefore our results have

ABSTRACT We propose that lateral heterostructures of single-atomic-layer graphene and hexagonal boron–carbon-nitrogen (hBCN) domains, can represent a powerful platform for the fabrication and the technological exploration of real two-dimensional field-effect transistors. Indeed, hBCN domains have an energy bandgap between 1 and 5 eV, and are lattice-matched with graphene; therefore they can be used in the channel of a FET to effectively inhibit charge transport when the transistor needs to be switched off. We show through *ab initio* and atomistic simulations that a FET with a graphene-hBCN-graphene heterostructure in the channel can exceed the requirements of the International Technology Roadmap for Semiconductors for logic transistors at the 10 and 7 nm technology nodes. Considering the main figures of merit for digital electronics, a FET with gate length of 7 nm at a supply voltage of 0.6 V exhibits I_{on}/I_{off} ratio larger than 10^4, intrinsic delay time of about 0.1 ps, and a power-delay-product close to 0.1 nJ/m. More complex graphene–hBCN heterostructures can allow the realization of different multifunctional devices, translating on a truly two-dimensional structure some of the device principles proposed during the first wave of nanoelectronics based on III–V heterostructures, as for example the resonant tunneling FET.
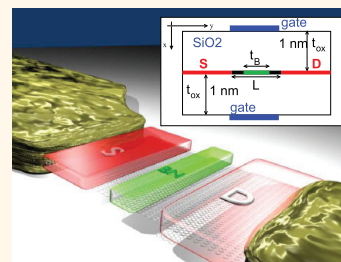
to be considered the upper limit of achievable performance.

RESULTS

The first device we propose is a double-gate FET with a channel consisting of a single-atomic-layer graphene-hBCN–graphene heterostructure, illustrated in Figure 1. The hBCN region, of length t_B, is exactly below the gates, and acts as the barrier for carrier flow. Two metallic gates have a length $L > t_B$ and therefore overlap on the graphene regions, and are separated from the channel by a silicon oxide layer of thickness 1 nm. Graphene regions below the gate are undoped, whereas those forming the source and drain extensions are doped with donors or acceptors for obtaining nFETs or pFETs, respectively. The doping

molar fraction f represents the number of doping atoms over the total number of carbon atoms in the contact extensions.

For the hBCN region we have considered four different materials: boron-nitride (BN), two different configurations with 50% concentration of carbon atoms (BC_2N and BC_2N', respectively) and 75% concentration of carbon atoms (BC_6N). Corresponding structures and energy dispersions are shown in Figure 2.

For an accurate computation of transport through the hBCN region, we need to extract parameters associated with the graphene/hBCN barrier height, especially electron affinity χ and the energy bandgap E_{gap}. Since they are not available in the literature, we have obtained them directly through *ab initio* simulations.

If the intrinsic Fermi level of graphene is considered as the reference potential (equal to zero) and $\chi_G = 4.248$ eV is the graphene electron affinity, the barrier heights seen by electron and holes read

$$BC = \chi_G - \chi \qquad (1)$$

and

$$BV = |\chi_G - \chi - E_{gap}| \qquad (2)$$

respectively, as illustrated in Figure 3.

Table 1 shows the main electronic properties extracted from DFT calculations, for different hBCN composites. As usual in the DFT framework, the electron affinity of an extended system is defined as the difference between the vacuum energy level and the
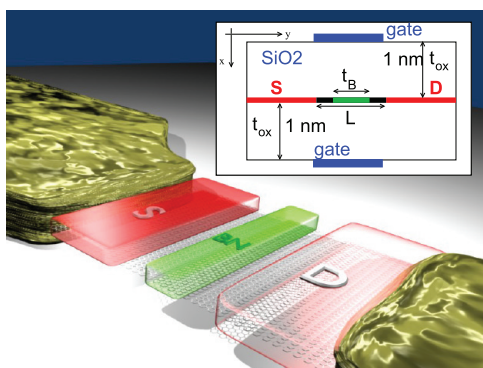

Figure 1. Graphene-based transistor with BN barrier in the channel (top and bottom gates are not depicted). In the inset, a longitudinal cross-section of the device is shown. Top and bottom oxides thickness $t_{ox} = 1$ nm. Source and drain reservoirs are 10-nm long with a molar fraction f, t_B is the barrier thickness, and L is the channel length.

Figure 3. Illustration of the band edge structure of the graphene/hBCN/graphene system for a zero potential. BC (BV) represents the difference between the conduction (valence) band of the barrier and the intrinsic Fermi level in graphene.
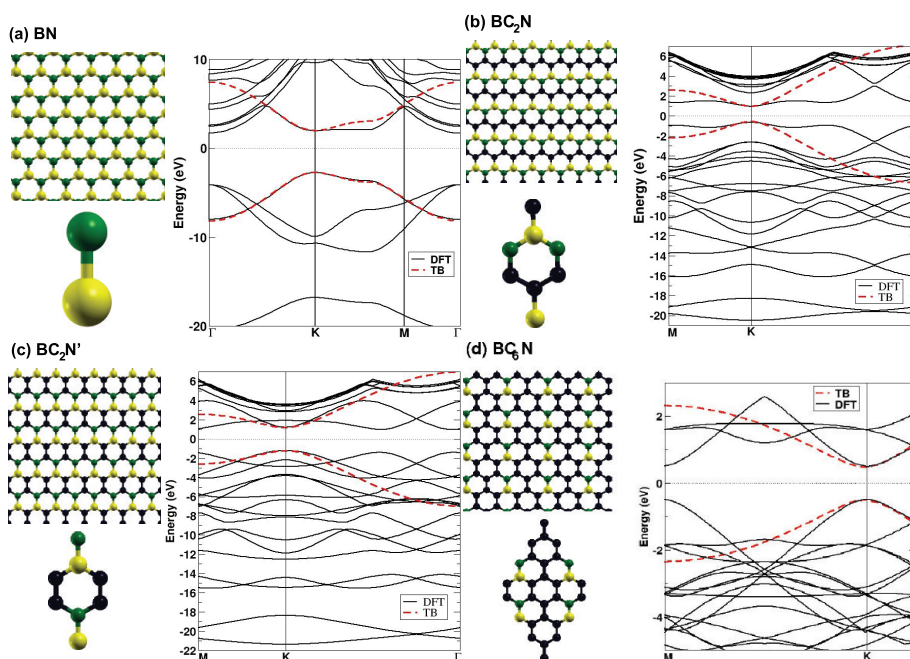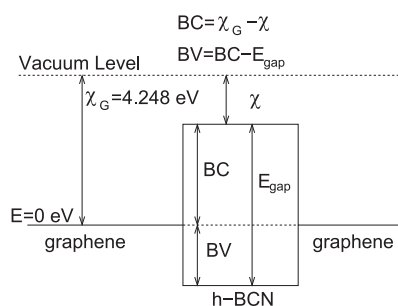

Figure 2. hBCN materials. For each material, the primitive cell and the bands computed by means of DFT-GGA simulations are shown. Dashed red lines refer to the bands computed by means of the tight-binding approach. The zero energy value indicates the Fermi level.

conduction band minimum level. In particular, experimental reports of the bandgap of h-BN range from 3.0 to 7.5 eV.[7] Related to this, the electron affinity is not uniquely determined. For each material, tight-binding parameters for a simple nearest-neighbor single-orbital Hamiltonian have been extracted consistently with results from *ab initio* simulations.

As can be seen in Figure 2, the bands obtained by means of the tight-binding approach are in good

TABLE 1. Electron Affinity (χ), Energy Gap (E_{gap}), and Barrier Height for Electrons (BC) and Holes (BV) for Two-Dimensional Composite Materials hBCN

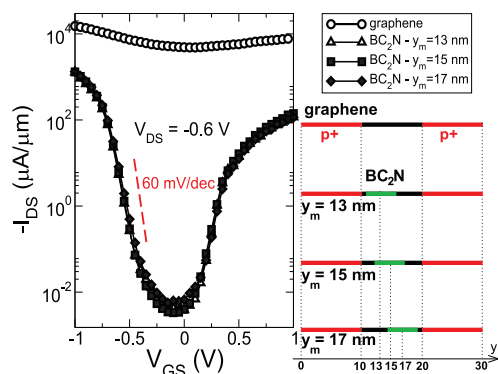| material	χ (eV)	E_{gap} (eV)	BC (eV)	BV (eV)
BN	1.11	4.70	3.137	1.563
BC_2N	3.30	1.59	0.948	0.642
BC_2N'	3.64	2.36	0.608	1.752
BC_6N	3.70	0.98	0.548	0.432

Figure 4. Transfer characteristics for the BC_2N FET for V_{DS} = 0.6 V, considering different values of y_m, *i.e.*, the coordinate of the middle of the hBCN region; t_B = 5 nm and $f = 10^{-2}$.

agreement with those computed through DFT calculations. In particular, the computed barriers in the conduction and valence bands (BC and BV, respectively) represent the on-site energies imposed in correspondence of the odd and even atoms of h-BCN material: such assumption reproduces the same E_{gap} and barrier height as DFT calculations. For what concerns instead the hopping parameters, we have assumed a parameter $t_1 = -2.59$ eV between atoms belonging to graphene regions, and $t_2 = -2.28$ eV for atoms belonging to the h-BCN barrier. The extracted parameters for the bandgap are in good agreement with recently published results.[8]

Since the barrier seen by holes is smaller than that seen by electrons in both BC_2N, BC_6N, and BN, we have simulated pFETs. For the BC_2N' instead, we have simulated an nFET. In Figure 4, we show the transfer characteristics of a device with BC_2N barrier for different positions y_m of the middle of the barrier along the longitudinal direction, when applying a supply voltage V_{DD} equal to 0.6 V. From the transfer characteristics when the voltage between drain and source is equal to the supply voltage V_{DD} one can extract one of the main figures of merit for digital logic: the I_{on}/I_{off} ratio, that is, the maximum ratio between the drain currents obtained by varying the voltage between gate and source (V_{GS}) by a quantity equal to the supply voltage V_{DD}. As can be seen, device behavior is extremely robust with respect to a variation of y_m, meaning that a perfect alignment of the hBCN region and metal gates is not required. In all cases the characteristics are almost identical, and an I_{on}/I_{off} ratio larger than 10^4 is obtained. Such robustness is remarkable considering graphene-based transistors: for example, one of the main problems of graphene nanoribbon transistors is that the gap has an extreme sensitivity to the variation
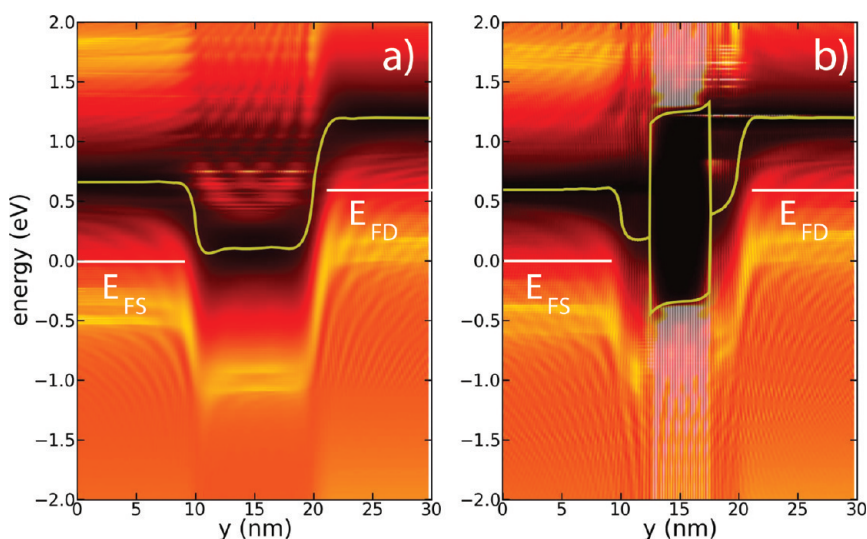

Figure 5. Local density of states (LDOS) for (a) graphene and (b) BC_2N p-MOS FET. The intrinsic Fermi level and the conduction and valence bands are depicted for the graphene and BC_2N device, respectively. E_{FS} (E_{FD}) is the Fermi level in the source (drain) reservoir. Brighter colors correspond to higher LDOS values.
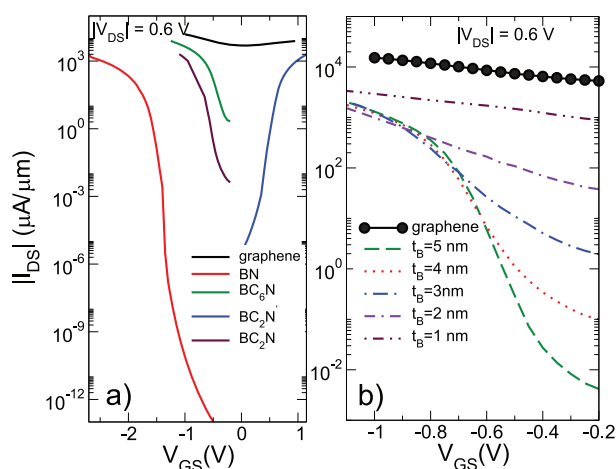
Figure 6. (a) Transfer characteristics for the different barrier materials. All the considered devices are p-type except BC2N'. Molar fraction $f = 10^{-2}$ for BC_2N, BC_2N', and BC_6N, while $f = 5 \times 10^{-2}$ for BN; $t_B = 5$ nm. (b) Transfer characteristics for the BC_2N device for different barrier length t_B and $y_m = 15$ nm. In both pictures, the transfer characteristic of a FET with a graphene-only channel at $V_{DS} = 0.6$ V is shown as a reference.

of just one dimer in the nanoribbon width, which in turn translates in an extreme sensitivity of the device characteristics.[4]

In the same Figure, we also show as a reference the transfer characteristics of a FET with a same geometry but with a pure graphene channel, exhibiting—as expected—an I_{on}/I_{off} ratio smaller than 10.

In Figure 5, the Local Density of States (LDOS) for a graphene FET and a graphene/BC_2N FET are shown for $V_{GS} = -0.3$ V: brighter colors correspond to higher LDOS values. In the graphene FET, small values of LDOS are in correspondence of the intrinsic Fermi level along the device. As can be seen in Figure 5a, the strong band-to-band tunneling component due to the zero bandgap leads to occupied states in the channel, degrading the electrostatic control of the gate over the channel barrier. In the BC_2N device instead, Figure 5b, apart from the small LDOS corresponding to the source and drain graphene reservoirs, a band gap can be clearly seen corresponding to the hBCN region, which blocks transport of electrons injected from the drain.

Let us notice that despite the double-gate structure and the very thin dielectric, the subthreshold swing (SS) is quite good (~80 mV/dec), but not ideal (60 mV/dec). This can be explained by the induced localized states corresponding to the drain. As can be seen in Figure 5a, a roughly triangular well is seen by electrons at the interface of the BC_2N barrier and the doped drain reservoir. Such states are negatively charged, since holes tunnel through the almost transparent barrier toward the drain, leaving an electron in the channel. In order to reduce such a charge, thicker barriers can be considered. However, it is important not to put the barrier in direct contact with the reservoirs, since problems may arise due the formation of a Schottky-like contact, which could further reduce the gate control over the channel barrier.

TABLE 2. Channel Length (L), I_{off}, I_{on}, I_{on}/I_{off} Ratio, Subthreshold Swing (SS), Power Delay Product (PDP) and Intrinsic Device Speed (τ) for the Different Simulated Devices

material	L (nm)	I_{off} (μA/μm)	I_{on} (μA/μm)	I_{on}/I_{off}	SS (mV/dec)	PDP (J/m)	τ (ps)
BC_2N	10	0.1	1736	17360	80	1.01×10^{-10}	0.097
BC_2N	7	0.1	1600	16000	83	7.84×10^{-11}	0.0817
BC_6N	10	2.15	2143	996	116	1.44×10^{-10}	0.112
BC_6N	7	2.55	2048	804	123	9.23×10^{-11}	0.0751
BC_2N'	10	0.1	1368	13678	66	1.22×10^{-10}	0.149
BC_2N'	7	0.1	1285	12850	67	8.08×10^{-11}	0.105
BN	10	0.1	491	4910	70	2.82×10^{-10}	0.96

Since a larger gap is typically correlated with a lower mobility, the graphene—hBCN—graphene heterostructure has also the advantage of confining the low mobility material to the tiny region of the channel barrier, whereas the high mobility material is used for the relatively longer source and drain extensions. In particular, we have verified[9] that the mean free path when considering electron—phonon interaction is of the order of tens of nanometers. Since the simulated barriers are equal to 5 nm, we can reasonably assume that phonon scattering is negligible in the considered devices. This is a significant advantage with respect to a FET with a channel of homogeneous hBCN.

In Figure 6a, we show the transfer characteristics for all the considered devices for $V_{DS} = 0.6$ V. Owing to the large BN barrier height, BN devices have a larger threshold voltage, and smaller I_{on}, but an SS similar to those obtained for the other devices. The transfer characteristics of a BC_2N FET for different values of t_B are shown in Figure 6b. As can be seen, as long as the length of the hBCN region is reduced, the overlap between gate and graphene increases, thereby increasing the channel quantum capacitance, and the subthreshold behavior is degraded.
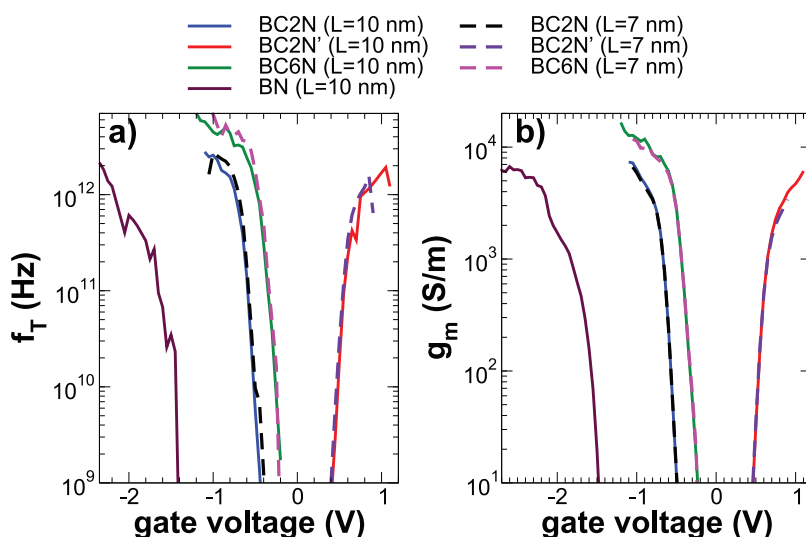
Figure 7. (a) Cut-off frequency defined as $f_T = g_m/2\pi C_G$, where g_m is the device transconductance and C_G is the gate capacitance, as a function of V_{GS} for the different hBCN barriers. (b) g_m as a function of V_{GS} for the different hBCN barriers.

In Table 2, we show the main figures of merit of FET performance. In addition to the I_{on}/I_{off} ratio that we have already considered, the intrinsic delay time τ and the power-delay product PDP are defined as:

$$\tau = \frac{C_G V_{DD}}{I_{on}} \quad (3)$$

$$PDP = V_{DD} I_{on} \tau \quad (4)$$

where C_G is the differential gate capacitance, computed as the derivative of the charge Q in the whole device for $V_{DS} = V_{DD}$, with respect to V_{GS}. As can be seen, BC$_2$N and BC$_2$N' FETs exhibit I_{on}/I_{off} larger than 10^4, meeting ITRS requirements.

To investigate the RF performance, we have computed with a quasi-static model the intrinsic cutoff frequency f_T, which reads

$$f_T = \frac{g_m}{2\pi C_G} \quad (5)$$

where g_m is the transconductance, defined as the derivative of I_D with respect to V_{GS}. Results are shown in Figure 7a, where f_T reaches the THz range. In Figure 7b the transconductance g_m is shown as a function of the gate voltage.

Using more complex heterostructures, devices with additional functionalities can be obtained. For example, we can obtain a resonant tunneling (RT) FET, simply using a channel with a graphene–BN–graphene–BN–graphene heterostructure below the two metal gates. The device is illustrated in Figure 8: the BN regions have a length t_B, where as the central graphene region (acting as the quantum well) has a length w. The rest is equal to the previously considered FET.

In this case the two barriers form a Fabry–Perot resonator for charge carriers that can be modulated in
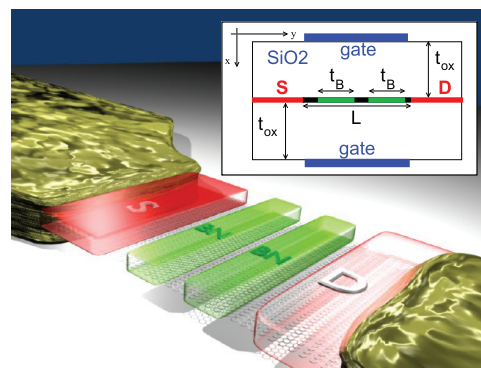

Figure 8. Illustration of the resonant tunneling FET with double BN barriers in the channel. In the inset, the longitudinal cross-section of the device is shown.

energy through the gate voltage. This introduces a negative transconductance region as shown in Figure 9a. As can be seen, the thinner the field oxide, the larger the gate control over the channel barrier, and the steeper the regions where negative differential transconductance appears.

In Figure 9b, the LDOS is shown for $V_{GS} = 0.5$ V. As can be seen, localized states appear in the quantum well (central graphene region) and are shifted upward or downward through the gate voltage. Whenever a resonant state aligns with the Fermi level of the source, a peak appears in the I_D–V_{GS} characteristics. Simulations assume here fully coherent transport, and therefore we can expect slightly reduced peak-to-valley ratios in the transfer characteristics due to phonon scattering and rough lateral heterostructure interfaces.

The real advantage of the proposed RT-FET over previous different proposals of resonant tunneling transistors, such as those based on III–V material systems,[10] is the extremely good electrostatic control of
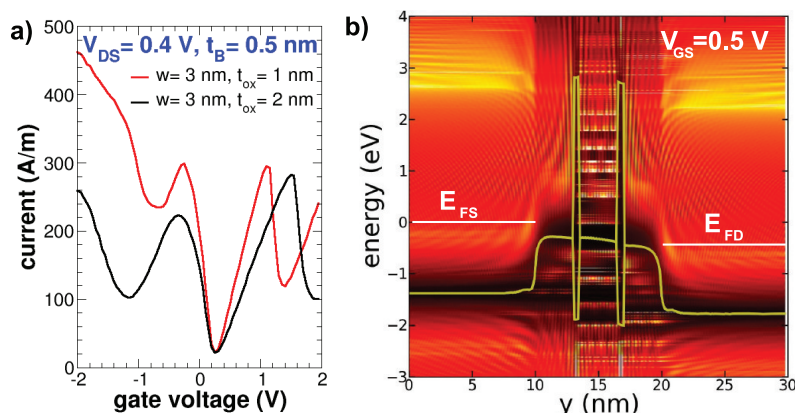
Figure 9. (a) I_{DS} vs V_{GS} for a device with a BN double barrier with the same t_B and $w = 3$ nm. Two different values of t_B have been considered. (b) LDOS for $V_{GS} = 0.5$ V.
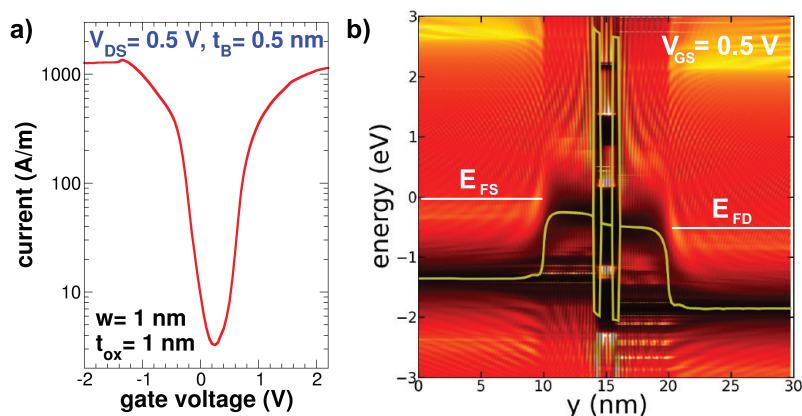

Figure 10. (a) I_{DS} vs V_{GS} for a device with a BN double barrier. Each barrier is 0.5 nm thick and the central region is 1 nm wide (w). (b) LDOS for $V_{GS} = 0.5$ V.

the devices, due to the truly flat channel, and the very efficient gate coupling to the channel, unachievable with bipolar operation and vertical heterostructures.

A different effect can be seen in the case of Figure 10a,b, where we consider a very narrow well: no negative transconductance appears, but resonance highly increases the current at smaller V_{GS} as compared to single barrier case.

CONCLUSION

We have shown that hybridized graphene with intercalated carbon and hBCN represents an exceptional platform for exploring truly two-dimensional nanoelectronics. The possibility to engineer the electronic properties of the channel with hBCN allows the acquisition of high I_{on}/I_{off} graphene-based FETs. For more complex heterostructures, devices with additional functionalities can be obtained. For example, a double BN barrier in the channel can be used for obtaining resonant tunneling FETs with extremely good gate control, interesting for beyond CMOS applications. We believe that the proposed structures represent a viable option to obtain graphene-based transistor suitable for digital logic.

COMPUTATIONAL METHODS

Ab initio calculations have been performed by means of the Quantum Espresso[11] code, using a plane wave basis set in the generalized gradient approximation (GGA) with the Perdew—Burke—Ernzerhof (PBE) exchange correlation functional. A 50 Ry wave function cutoff and 400 Ry charge density cutoff have been considered, while the Brillouin zone has been sampled using a $30 \times 30 \times 2$ Monkhorst—Pack grid. A 30 bohr layer of vacuum is considered to separate the sheet from its periodical images, which we have verified to be sufficient to avoid any unphysical interactions. The geometries are fully relaxed without any symmetry constraints, while the convergence of total energy and force are set to 1×10^{-7} Ry/au

The obtained energy dispersion relations have been then fitted to extract tight-binding parameters and to accurately reproduce the bottom conduction band and the top valence band. To this purpose, our open-source device simulation package NanoTCAD ViDES[12] has been extensively exploited to evaluate device operation through the self-consistent solution of the 2D Poisson and the Schrödinger equation with open boundary conditions, within the non-equilibrium Green's function (NEGF) formalism.

In particular, we have described the Hamiltonian for the considered two-dimensional material taking into account Bloch periodic boundary conditions along the transversal direction with period $\Delta = 3a_{cc}$, where $a_{cc} = 0.144$ nm is the carbon—carbon bonding distance,[13,14] which leads to a k_x wave vector dependence in the Hamiltonian. Semi-infinite contacts have been modeled along the longitudinal direction by means of self-energies.

Conflict of Interest: The authors declare no competing financial interest.

REFERENCES AND NOTES

1. Lemme, M.; Echtermeyer, T.; Baus, M.; Kurz, H. A Graphene Field-Effect Device. *IEEE Electron Device Lett.* **2007**, *28*, 282–284.
2. Avouris, P.; Chen, Z.; Perebeinos, V. Carbon-Based Electronics. *Nat. Nanotechnol.* **2007**, *2*, 605–615.
3. Schwierz, F. Graphene Transistors. *Nat. Nanotechnol.* **2010**, *5*, 487–496.
4. Fiori, G.; Iannaccone, G. Simulation of Graphene Nanoribbon Field-Effect Transistors. *IEEE Electron Device Lett.* **2007**, *28*, 760–762.
5. Iannaccone, G.; Fiori, G.; Macucci, M.; Michetti, P.; Cheli, M.; Betti, A.; Marconcini, P. Perspectives of Graphene Nanoelectronics: Probing Technological Options with Modeling. *Proc. Int. Electron Device Meet.* **2009**, 245–248.
6. Ci, L.; Song, L.; Jin, C.; Jariwala, D.; Wu, D.; Li, Y.; Srivastava, A.; Wang, Z. F.; Storr, K.; L. Balicas, P. M. A.; Liu, F. Atomic Layers of Hybridized Boron Nitride and Graphene Domains. *Nat. Mater.* **2010**, *9*, 430–435.
7. Ooi, N.; Rairkar, A.; Lindsley, L.; Adams, J. B. Electronic Structure and Bonding in Hexagonal Boron Nitride. *J. Phys. Condens. Matter* **2006**, *18*, 97–115.
8. Zhu, J.; Bhandary, S.; Sanyal, B.; Ottosson, H. Interpolation of Atomically Thin Hexagonal Boron Nitride and Graphene: Electronic Structure and Thermodynamic Stability in Terms of All-Carbon Conjugated Paths and Aromatic Hexagons. *J. Phys. Chem. C* **2011**, *115*, 10264–10271.
9. Bruzzone, S.; Fiori, G. *Ab-Initio* Simulations of Deformation Potentials and Electron Mobility in Chemically Modified Graphene and Two-Dimensional Hexagonal Boron—Nitride. *Appl. Phys. Lett.* **2011**, *99*, 222108.
10. Capasso, F.; Sen, S.; Gossard, A.; Hutchinson, A.; English, J. Quantum Well Resonant Tunneling Bipolar Transistor Operating at Room Temperature. *Proc. Int. Electron Device Meet.* **1986**, 282–285.
11. Giannozzi, P.; Baroni, S.; Bonini, N.; Calandra, M.; Car, R.; Cavazzoni, C.; Ceresoli, D.; Chiarotti, G. L.; Cococcioni, M.; Dabo1, I.; *et al.* QUANTUM ESPRESSO: A Modular and Open-Source Software Project for QuantumSimulations of Materials. *J. Phys.: Condens. Matter* **2009**, *21*, 395502.
12. Available at: http://www.nanohub.org/tools/vides. DOI: 10254/nanohub-r5116.5 (Accessed July 8, 2009).
13. Fiori, G.; Iannaccone, G. On the Possibility of Tunable-Gap Bilayer Graphene. *IEEE Electron Device Lett.* **2009**, *30*, 261–264.
14. Fiori, G.; Iannaccone, G. Ultralow-Voltage Bilayer Graphene Tunnel FET. *IEEE Electron Device Lett.* **2009**, *30*, 1096–1098.